

An Integrated Framework for Obstacle Mapping with See-Through Capabilities using Laser and Wireless Channel Measurements

Alejandro Gonzalez-Ruiz, Alireza Ghaffarkhah, Yasamin Mostofi

Abstract – In this paper we consider a team of mobile robots that are tasked with building a map of the obstacles, including occluded ones, in a given environment. We propose an integrated framework for mapping with see-through capabilities using laser and wireless channel measurements, which can provide mapping capabilities beyond existing methods in the literature. Our approach leverages the laser measurements to map the visible parts of the environment (the parts that can be sensed directly by the laser scanners) using occupancy grid mapping. The parts that can not be properly mapped by laser scanners (e.g. the occluded parts) are then identified and mapped based on wireless channel measurements. For the latter, we extend our recently-proposed wireless-based obstacle mapping framework to a probabilistic approach by utilizing Bayesian Compressive Sensing (BCS). We further consider an integrated approach based on using Total Variation (TV) minimization. We compare the performance of our two integrated methods, using both simulated and real data, and show the underlying tradeoffs. Finally, we propose an adaptive path planning strategy that utilizes the current estimate of uncertainty to collect wireless measurements that are more informative for obstacle mapping. Overall, our framework enables mapping occluded structures that can not be mapped with laser scanners alone or a small number of wireless measurements. Our experimental robotic testbed further confirms that the proposed integrated framework can map a more complex real occluded structure that can not be mapped with existing strategies in the literature.

I. INTRODUCTION

Mobile robotic networks can play a key role in areas such as emergency response, surveillance and security, and battlefield operations. In order for a mobile robotic network to operate autonomously, accurate mapping of obstacles/objects is essential. The obstacle/object map can be a 2D (or 3D) grid map of the environment, where we have zeros at locations where there is no obstacle and non-zero values at obstacle locations.

In the robotics community, the problem of mapping has been widely explored [1]–[4]. Depending on whether the positions and orientations of the robots are known, the mapping problem can be tackled using different approaches. In mapping with known poses, for instance, occupancy grid mapping approaches [1], [5] have been proposed to build a grid map of the obstacles by sequentially updating the posterior of having an obstacle in each cell of the grid based on the new set of sensory (sonar or laser) measurements. In most of the current work on occupancy

grid mapping, the cells are assumed statistically independent. Although this assumption is reasonable for high-quality sensory data such as laser, it results in a poor performance when the occupancy grid approach is applied to low-quality data such as sonar. One of the few works that considers the correlation of the cells to deal with low-quality sonar data is [6]. In this work, the authors propose using polygonal random fields to model the correlation of the cells.

For mapping with unknown poses, the simultaneous localization and mapping (SLAM) approaches are used to incrementally build a map of the environment, while estimating the location of the robot within the map [3], [4], [7]–[9]. The SLAM problem is among the most challenging problems in autonomous robotics. Several techniques based on using extended Kalman filters (EKF) [10] and Rao-Blackwell particle filters [11]–[14] have been proposed by the researchers to solve this problem. Both occupancy grid maps and landmark-based maps (a set of known landmarks in the environment) can be considered in SLAM, depending on the utilized algorithm and the type of the environment [3].

In the current mapping approaches using sonar/laser sensors, only areas that are directly sensed by the sensors are mapped [1]–[4]. In several scenarios, it may be necessary to further have *see-through capabilities* and map the objects that can not be directly sensed. For instance, the robots may need to build an understanding of the objects inside a room, before entering it. Having see-through capabilities can also reduce the overall mapping time and energy in any networked robotic operation. In general, devising see-through mapping strategies, i.e., mapping without direct sensing, can be considerably challenging.

In our previous work [15]–[19], we proposed a framework for see-through mapping based on using very few wireless channel measurements. In order to extract the obstacle information, without making a prohibitive number of wireless transmissions, we utilized the recent results in the area of compressive sensing (CS) [20], [21]. In [15], [16], we showed how an obstacle map can be reconstructed with very few wireless samples by exploiting the sparse representation of the map in a transform domain such as wavelet. In [17], [18], we proposed two sampling strategies for compressive obstacle mapping, namely wireless coordinated measurements and wireless random measurements. We used the fact that the gradient of an obstacle map is sparse and reconstructed the map by minimizing its total variation (TV). In [18] we showed the underlying tradeoffs of different sampling strategies, reconstruction techniques, and sparsity domains for compressive wireless-based obstacle mapping. Wireless measurements have

This work is supported in part by NSF CAREER award #0846483.

The authors are with the Department of Electrical and Computer Engineering, University of California Santa Barbara, Santa Barbara, CA 93106, USA email: {agon, alinem, ymostofi}@ece.ucsb.edu.

also been utilized for detection and tracking of moving objects [22], [23].

In our past work, we showed the performance of our wireless-based obstacle mapping in reconstructing simple occluded structures [16]–[19]. In general, however, obstacle mapping of more complicated structures, solely based on wireless measurements, is extremely challenging due to all the propagation phenomena. Obstacle mapping based on laser scanner data, on the other hand, can typically detect the visible objects with a good accuracy but has no see-through capability.

The main goal of this paper is then to develop an integrated framework that keeps the benefits of both laser-based (or sonar-based) and wireless-based mapping approaches for the reconstruction of more complex occluded structures. Our proposed approach integrates occupancy grid mapping with compressive sensing to fuse the laser and wireless channel measurements. In order to do so, we utilize some of the recent results in the area of probabilistic compressive sensing, i.e. Bayesian Compressive Sensing (BCS) [24], [25]. The goal of Bayesian Compressive Sensing (BCS) is to reconstruct the signal by using a prior probability distribution that preserves the sparsity [26]. A valuable property of the BCS approach is that it also provides a posterior belief of the signal of interest (an estimated variance). Therefore, it is possible to calculate a measure of uncertainty for the estimation of each cell, which is not possible using traditional CS methods. This property of BCS makes it a potential candidate for probabilistic obstacle mapping, as it is more informative in general or can specifically be used for online adaptive data collection. However, the applicability of BCS approach for see-through mapping of real obstacles, based on wireless measurements, has not been studied before. Therefore, we first develop an integrated grid mapping and BCS-based approach for mapping of occluded structures.

We further show how the estimated variance of the BCS approach can be utilized to devise adaptive online data collection strategies that guide the robots to make wireless measurements at positions that minimize the uncertainty of the estimated map. For the sake of completion, we also show how to integrate occupancy grid mapping with the existing TV-based wireless mapping approach of [18]. Along this line, we compare the performance of our BCS-based and TV-based integrated approaches and shed light on the underlying tradeoffs. We shall see that the BCS-based mapping approach relies on an initial estimation of the underlying model parameters, which requires some form of a priori measurements and can be prone to error propagation. On the other hand, having an assessment of uncertainty can be useful for several applications. Thus, it is worth studying both BCS-based and TV-based integrated approaches since a given scenario may favor one over the other.

We next briefly summarize the main contributions of this paper:

- 1) We propose an integrated occupancy grid and wireless-based CS approach for see-through obstacle mapping. We show that our integrated framework can map occluded structures that can not be mapped solely based on either approaches. More specifically, we show how both BCS and TV minimization can be integrated with occupancy grid mapping and shed light on the underlying tradeoffs using both simulated and real data that is collected with

our robotic platforms. Our results indicate that our integrated TV-based approach works better when coordinated wireless measurements can be gathered while BCS-based approach has an advantage with random (unstructured) measurements. Unstructured measurements may be the only option in several scenarios due to environmental constraints.

- 2) We devise an adaptive path planning and data collection framework that uses the current estimate of uncertainty to improve the see-through performance of our integrated framework.
- 3) We implement the proposed approach on our robotic platforms. The main experimental result of the paper (Fig. 13), for instance, shows how our proposed approach can map structures that can not be mapped with any of the existing approaches in the literature.

The rest of the paper is organized as follows. In Section II, we introduce our system model. In Section III, we provide a brief summary of the occupancy grid mapping. The occupancy grid mapping is then integrated with BCS in Section IV and with TV minimization in Section V. We discuss the underlying tradeoffs of different sampling strategies using BCS and TV minimization in Section VI. Our adaptive path planning and data collection strategy is then introduced in Section VII. We present our experimental results in Section VIII and conclude in Section IX.

II. SYSTEM MODEL

Consider the case that a workspace $\mathcal{W} \subset \mathbb{R}^2$ needs to be mapped by a team of m mobile robots.¹ We discretize \mathcal{W} into n small non-overlapping cells. The map of the workspace then refers to a binary vector $x = [x_1, \dots, x_n]^T$, where $x_k = 1$ if there is an obstacle in the k^{th} cell in the workspace, and $x_k = 0$ otherwise. In this paper, we consider building a 2D map of the obstacles. This means that for real 3D structures, we reconstruct a horizontal cut of them.

Each mobile robot is equipped with a laser scanner, a wireless communication device (e.g. a IEEE 802.11 WLAN card) and a directional antenna. The robots collect two sets of measurements: laser measurements and wireless channel measurements, i.e. the received signal strength indicator (RSSI) between different pairs of robots. For the purpose of making pair-wise channel measurements, for each pair of TX-RX robots, the receiving robot measures the received signal strength (RSSI value) from the transmission of the transmitting robot. A schematic of the mapping scenario considered in this paper is shown in Fig. 1.

Note that the trajectories of the robots when taking the laser measurements may not be the same as their trajectories when taking the wireless channel measurements. In other words, the laser and wireless channel measurements could be available from two different sets of trajectories for the robots.

¹Although for our experiments we use only two mobile robots, the proposed mapping framework of this paper is applicable to more than two robots. We, therefore, introduce our framework for a team of m robots that cooperate to map the workspace. However, we assume that measurement collection is coordinated (or is done serially) such that different transmissions are not interfering with each other.

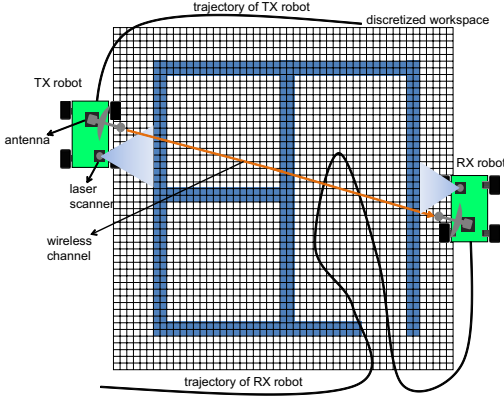


Fig. 1. Schematic of the proposed integrated mapping scenario using laser and wireless channel measurements.

A. Laser Measurement Model

Let $z_{i,t}$ denote the laser measurement of the i^{th} mobile robot at time step t .² Furthermore, let $q_{i,t} = (\xi_{i,t}, \theta_{i,t})$, for $\xi_{i,t} \in \mathcal{W}$ and $\theta_{i,t} \in (-\pi, \pi]$, represent the position and orientation of the i^{th} mobile robot at time step t when taking the laser measurement. We show by z_t and q_t the stacked vectors of $z_{i,t}$ and $q_{i,t}$ of all the robots at time t , respectively. The stacked vectors of z_t and q_t from time step 1 to time step t are also shown by $z_{1:t}$ and $q_{1:t}$, respectively.

By the laser measurement model, we mean the probabilistic model that relates $z_{i,t}$ and $q_{i,t}$ to the map x at any time t . In the robotics literature, this model is generally found empirically and is given in two different ways. The *forward* measurement model for laser scanners gives $p(z_{i,t}|x, q_{i,t})$, i.e., the probability density function (pdf) of $z_{i,t}$ conditioned on x and $q_{i,t}$ [1]. The *reverse* measurement model, on the other hand, gives $p(x_k|z_{i,t}, q_{i,t})$, i.e., the probability of the presence or absence of an obstacle in the k^{th} cell conditioned on $z_{i,t}$ and $q_{i,t}$ [1]. The probability $p(x|z_{i,t}, q_{i,t})$ is then calculated assuming independent x_k : $p(x|z_{i,t}, q_{i,t}) = \prod_{k=1}^n p(x_k|z_{i,t}, q_{i,t})$.

In Section III, we summarize how the forward or reverse measurement models can be used to calculate the map posterior probability, i.e., the posterior probability of having an obstacle in each cell, at any time t . The map posterior can then be used to find the cells that have not been scanned efficiently by the onboard laser scanners of the robots up to time t . After using all the collected laser measurements of the robots, x_k for such cells are estimated based on the wireless channel measurements in our proposed integrated framework. In this framework, we integrate occupancy grid mapping with Bayesian compressive sensing (BCS) and TV minimization to map the parts of the map that could not be seen by the laser scanners of the robots. These two methods are explained in Sections IV and V, respectively.

B. Wireless Channel Measurement Model

In addition to the laser measurements, the robots also take a set of wireless channel measurements. These measurements can be collected while the robots take the laser measurements or after taking the laser measurements along a different set of trajectories. Let $y_{i,j,t}$ denote the RSSI measurement between the i^{th} robot as the transmitter (TX) and the j^{th} one as the receiver

(RX) at time t .³ In the wireless communication literature, it is well established that $y_{i,j,t}$ can be characterized by a non-stationary stochastic process with three dynamics: *path loss*, *shadowing* and *multipath fading*. Path loss refers to the distance-dependent power fall-off. Shadowing or shadow fading is due to blockage of the transmitted signal by the obstacles and, therefore, contains implicit information of the obstacles along the communication path. Multipath fading is caused by multiple replicas of the transmitted signal that reach the antenna of the RX robot with different delays and phases [27]. We then have the following for $y_{i,j,t}$, in the dB domain [27], [28]:

$$y_{i,j,t} = \underbrace{K_{i,j} - 10 \eta_{i,j} \log_{10} (\|\xi_{i,t} - \xi_{j,t}\|)}_{\text{path loss}} - \underbrace{\phi^T(\xi_{i,t}, \xi_{j,t}) \alpha}_{\text{shadowing}} + \underbrace{\omega_{i,j,t}}_{\text{multipath fading}}, \quad (1)$$

where $K_{i,j}$ and $\eta_{i,j}$ are the path loss coefficients for the channel between robots i and j . For the shadowing term, the vector α contains the exponential decay coefficients of the wireless signal at each cell. For each cell k , we have $\alpha_k = 0$ if $x_k = 0$, and $\alpha_k > 0$ otherwise. The k^{th} element of vector $\phi(\xi_{i,t}, \xi_{j,t})$ is the distance that the line segment between $\xi_{i,t}$ and $\xi_{j,t}$ travels across the k^{th} cell multiplied by $\log_{10} e$ (see [18] for details). As can be seen, shadowing characterizes wireless signal attenuation as it goes through the obstacles along the transmission path and therefore contains implicit information about the objects along that line. Finally, the term $\omega_{i,j,t}$ is a zero-mean random variable which captures the effects of multipath fading and other modeling errors.

In practice, the path loss parameters can be estimated through a few line-of-sight (LOS) transmissions in the same environment, as we have shown in [28], [29]. By subtracting the path loss terms from $y_{i,j,t}$ in (1), stacking up all the centered (unbiased) wireless measurements with an arbitrary order, and flipping the sign, we get the following:

$$\tilde{y} = \Phi \alpha + \omega, \quad (2)$$

where \tilde{y} is the stacked vector of the centered RSSI values, Φ is a matrix with its rows given by $\phi^T(\xi_{i,t}, \xi_{j,t})$, in the same order as the elements of \tilde{y} , and ω is the vector of zero-mean random variables $\omega_{i,j,t}$. In order to use the BCS method for estimating the decay coefficients in Section IV, we furthermore assume that the elements of ω are uncorrelated Gaussian random variables with the variance of σ_0^2 . This implies that the pdf of \tilde{y} conditioned on α , i.e., $p(\tilde{y}|\alpha)$, can be characterized by a multi-variate zero-mean Gaussian pdf with covariance matrix $\sigma_0^2 I_{n_w}$, for I_{n_w} denoting the n_w -dimensional identity matrix and n_w representing the number of total wireless channel measurements. Note that distributions such as Nakagami or Rayleigh may better characterize ω in non-dB domain [27]. However, [30] shows that a Gaussian distribution (in the dB domain) can also provide a good enough fit. We next assert this with our channel measurements in Fig. 2. In this experiment, we take the RSSI values of the wireless channel measurements between two robots (in the setup of Fig. 1) and subtract the

²For a typical laser scanner (e.g. SICK LMS laser range finders), $z_{i,t}$ is a vector of a fixed number of scalar range measurements.

³Note that the wireless channel measurements may not be available from every pair (i, j) . In other words, only a subset of robots may be used for channel measurements.

ideal measurements (in dB) to obtain the noise component as follows: $\omega = \tilde{y} - \Phi\alpha$. Fig. 2 then shows the distribution of this noise, which confirms that a Gaussian distribution can provide a good enough fit. The mean and standard deviation of this best fit are $\hat{\mu} = 0.22$ and $\hat{\sigma}_0 = 10.25$, respectively.

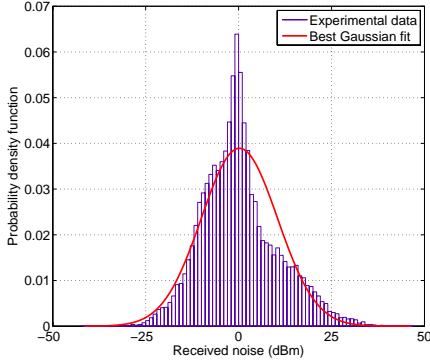


Fig. 2. The distribution of the noise (ω) of Eq. 2 from our experimental data and the corresponding best Gaussian fit ($\hat{\mu} = 0.22$ and $\hat{\sigma}_0 = 10.25$).

Note that vector α is related to the binary vector x . It is, however, a real vector as opposed to a binary one, as it shows the decay coefficients of the cells that contain obstacles. In Sections IV and V, we show how to estimate α , using BCS and TV minimization methods. Since the final goal is to estimate the binary vector x , the estimated α is then passed through a hard-limiter, as we further elaborate in Sections IV and V.

III. A BRIEF OVERVIEW OF OCCUPANCY GRID MAPPING USING LASER MEASUREMENTS

In the occupancy grid mapping, the goal is to calculate the map posterior probability, i.e., the probability of having an obstacle (or not) in any cell, conditioned on the laser and pose/odometry measurements. Depending on whether $q_{1:t}$ is available, the map posterior is found using two approaches: *mapping with known poses* and *mapping with unknown poses using SLAM*. Next we briefly explain both approaches. More detailed explanations can be found in [1], [3], [4].

Assume that x_k , for $k = 1, \dots, n$, are probabilistically independent. Also, assume no prior knowledge on the existence of an obstacle in each cell, i.e., $p(x_k = 1) = p(x_k = 0) = \frac{1}{2}$. In *mapping with known poses*, the map posterior of interest is $p(x_k|z_{1:t}, q_{1:t})$, which can be written as follows:

$$p(x_k|z_{1:t}, q_{1:t}) = \frac{p(z_t|x_k, q_t)p(x_k|z_{1:t-1}, q_{1:t-1})}{p(z_t|z_{1:t-1}, q_{1:t})},$$

$$p(z_t|x_k, q_t) = \prod_{i=1}^m \frac{p(x_k|z_{i,t}, q_{i,t})p(z_{i,t}|q_{i,t})}{p(x_k)}, \quad (3)$$

which results in

$$p(x_k|z_{1:t}, q_{1:t}) = \frac{\prod_{i=1}^m p(x_k|z_{i,t}, q_{i,t}) \prod_{i=1}^m p(z_{i,t}|q_{i,t})}{p(z_t|z_{1:t-1}, q_{1:t}) \prod_{i=1}^m p(x_k)} \times p(x_k|z_{1:t-1}, q_{1:t-1}). \quad (4)$$

In *mapping with unknown poses* the positions and orientation of the mobile robots are not given and the map posterior is found using the SLAM algorithm. Given only the laser measurements and the odometry inputs of the robots, the map posterior of interest is $p(x|z_{1:t}, u_{1:t-1})$ in this case, where $u_{1:t-1}$ is the stacked vector of the odometry inputs of the robots up to time $t - 1$. We next briefly summarize how $p(x|z_{1:t}, u_{1:t-1})$ can be

estimated using the well-known Rao-Blackwell particle filter (RBPF) for SLAM [3]. The RBPF for SLAM works based on the following factorization:

$$p(x|z_{1:t}, u_{1:t-1}) = \int \underbrace{p(x|z_{1:t}, q_{1:t})}_{\text{mapping with known poses}} \underbrace{p(q_{1:t}|z_{1:t}, u_{1:t-1})}_{\text{localization}} dq_{1:t}. \quad (5)$$

This integral is then approximated by the weighted sum of $p(x|z_{1:t}, q_{1:t})$ for a number of potential trajectories of the robots. Based on the Markovian property for the dynamical model of the robots, the pdf $p(q_{1:t}|z_{1:t}, u_{1:t-1})$ can be written as follows:

$$p(q_{1:t}|z_{1:t}, u_{1:t-1}) = p(q_t|q_{1:t-1}, z_{1:t}, u_{t-1})p(q_{1:t-1}|z_{1:t-1}, u_{1:t-2}) = \frac{p(z_t|q_{1:t}, z_{1:t-1})p(q_t|q_{t-1}, u_{t-1})}{p(z_t|z_{1:t-1}, u_{1:t-1})}p(q_{1:t-1}|z_{1:t-1}, u_{1:t-2}). \quad (6)$$

In RBPF for SLAM, the potential trajectories of the robots are represented by a number of particles. For each particle, an individual map posterior is built sequentially based on the new observations and the pose posterior estimates from the localization part. Assume L particles are used. Let $q_t^{[\ell]}$ denote the potential position and orientation of the robots at time t generated by the ℓ^{th} particle. The general form of the RBPF for SLAM is described by the following four steps [14]:

- 1) A proposal distribution $\pi(q_t|q_{1:t-1}^{[\ell]}, z_{1:t}, u_{t-1})$ is calculated for each particle ℓ . Then $q_t^{[\ell]}$ is found by sampling from this proposal distribution: $q_t^{[\ell]} \sim \pi(q_t|q_{1:t-1}^{[\ell]}, z_{1:t}, u_{t-1})$.
- 2) The weights of the particles are calculated as follows: $w_t^{[\ell]} = \frac{p(q_t^{[\ell]}|z_{1:t}, u_{1:t-1})}{\pi(q_t^{[\ell]}|z_{1:t}, u_{1:t-1})}$, which results in the following recursion for updating the weights based on (6):

$$w_t^{[\ell]} \propto \frac{p(z_t|q_{1:t}^{[\ell]}, z_{1:t-1})p(q_t^{[\ell]}|q_{t-1}^{[\ell]}, u_{t-1})}{\pi(q_t|q_{1:t-1}^{[\ell]}, z_{1:t}, u_{t-1})}w_{t-1}^{[\ell]}, \quad (7)$$

for $p(z_t|q_{1:t}^{[\ell]}, z_{1:t-1})$ given as follows: $p(z_t|q_{1:t}^{[\ell]}, z_{1:t-1}) = \sum_x p(z_t|x, q_t^{[\ell]})p(x|z_{1:t-1}, q_{1:t-1}^{[\ell]})$. The updated weights are normalized such that $\sum_{\ell=1}^L w_t^{[\ell]} = 1$.

- 3) The effective number of particles is calculated as $L_{\text{eff},t} = \left[\sum_{\ell=1}^L (w_t^{[\ell]})^2 \right]^{-1}$. If $L_{\text{eff},t} < L_{\text{th}}$, for a given threshold L_{th} , then resampling is performed. This is done by selecting L particles, with replacement, from the set of all the particles up to time t , with probability of selection proportional to $w_t^{[\ell]}$. The selected particles are given uniform weights of $\frac{1}{L}$.
- 4) For each particle, $p(x|z_{1:t}, q_{1:t}^{[\ell]})$ is found using mapping with known pose methods of the previous section. The final map posterior that is reported is then $\sum_{i=1}^L w_i^{[\ell]} p(x|z_{1:t}, q_{1:t}^{[\ell]})$.

Several proposal distributions have been utilized in the literature. For instance, the landmark-based FastSLAM 1.0 algorithm uses the motion model as the proposal: $\pi(q_t|q_{1:t-1}^{[\ell]}, z_{1:t}, u_{t-1}) = p(q_t|q_{t-1}^{[\ell]}, u_{t-1})$ [11]. The more updated FastSLAM 2.0 algorithm uses $\pi(q_t|q_{1:t-1}^{[\ell]}, z_{1:t}, u_{t-1}) = p(q_t|q_{1:t-1}^{[\ell]}, z_{1:t}, u_{t-1})$ [12]. An improved RBPF algorithm for

grids called *gmapping* uses a Gaussian approximation of the observation likelihood as the proposal distribution [14].

Let us define the quantity $\psi_{k,t}$ as follows: $\psi_{k,t} \triangleq \log \left(\frac{p(x_k=1|z_{1:t},u_{1:t-1})}{p(x_k=0|z_{1:t},u_{1:t-1})} \right)$. This way, $\psi_{k,t}$ represents a measure of certainty for any cell k at time t , independent of how the map posterior is calculated.

IV. INTEGRATION OF OCCUPANCY GRID MAPPING AND BAYESIAN COMPRESSIVE SENSING (BCS) FOR MAPPING WITH SEE-THROUGH CAPABILITIES

In this section, we show the implication of BCS [24], [25], [31] for the mapping of occluded structures and how it can be used to map the portion of the workspace that cannot be seen by the onboard laser scanners of the robots. BCS uses the fact that the vector α is sparse in the spatial domain. By applying Bayesian filtering methods and using a prior distribution for α that preserves its sparsity, BCS can effectively estimate α in places that cannot be seen by the laser scanners. Next we explain this method in more details.

Consider the partial map found using the laser measurements up to time t (in the middle or at the end of laser mapping operation). Define the following sets of indices: $\mathcal{I}_f \triangleq \{1 \leq k \leq n \mid \psi_{k,t} \leq -\psi_{\text{th}}\}$, $\mathcal{I}_o \triangleq \{1 \leq k \leq n \mid \psi_{k,t} \geq \psi_{\text{th}}\}$ and $\mathcal{I}_u \triangleq \{1 \leq k \leq n \mid |\psi_{k,t}| < \psi_{\text{th}}\}$, where $\psi_{\text{th}} > 0$ denotes a threshold. The sets \mathcal{I}_f and \mathcal{I}_o correspond to the indices of the cells that are estimated to be free-of-obstacle or occupied-by-obstacle, respectively. In other words, we have $\hat{x}_k = 0$ for $k \in \mathcal{I}_f$, and $\hat{x}_k = 1$ for $k \in \mathcal{I}_o$, where \hat{x}_k denotes the estimate of x_k . The cells whose indices are in \mathcal{I}_u are the unknown cells which could not be seen by the laser scanners. Note that laser scanners can typically provide a good mapping quality and, therefore, every cell k that has been seen by the laser scanner of one of the robots belongs to either \mathcal{I}_f or \mathcal{I}_o with a high probability.

Let us rearrange the elements of x as follows: $x = [x_f^T \ x_o^T \ x_u^T]^T$, where x_f , x_o and x_u denote the stacked vectors of the elements of x whose indices are in \mathcal{I}_f , \mathcal{I}_o and \mathcal{I}_u , respectively. Also let \hat{x}_f , \hat{x}_o and \hat{x}_u denote the vectors with the estimates of the elements of x corresponding to \mathcal{I}_f , \mathcal{I}_o and \mathcal{I}_u , respectively. Since x_f and x_o are already estimated well using laser scanners, i.e., all the elements of \hat{x}_f are set to zero and all the elements of \hat{x}_o set to one, the goal is then to estimate x_u using wireless channel measurements. Our strategy consists of two steps:

- 1) We first estimate the corresponding decay coefficients of the cells in \mathcal{I}_o and \mathcal{I}_u jointly, based on wireless channel measurements and assuming that decay coefficients of the cells in \mathcal{I}_f are zero.
- 2) Using the estimated decay coefficients of the cells in \mathcal{I}_u , we set $\hat{x}_k = 1$, for $k \in \mathcal{I}_u$, if the estimated decay coefficient of the k^{th} cell is larger than a threshold α_{th} , and $\hat{x}_k = 0$ otherwise.

Note that based on only laser measurements, the decay coefficients of the cells in \mathcal{I}_o are not known beforehand. We, therefore, need to estimate their decay coefficients together with the decay coefficients of the cells in \mathcal{I}_u in the first step. However, since these cells are already estimated to be occupied, we do not use their decay coefficients to detect their occupancy

in the second step, i.e. we impose the decision generated by the laser scanner for these cells.

Similar to vector x , let us also rearrange the elements of the decay coefficient vector α as $\alpha = [\alpha_f^T \ \alpha_o^T \ \alpha_u^T]^T$. We next show how to estimate $\alpha_{o,u} = [\alpha_o^T \ \alpha_u^T]^T$ using wireless channel measurements and Bayesian Compressive Sensing (BCS). Consider the stacked vector of the centered RSSI values \tilde{y} in Section II-B. Using the rearranged vector α , we get

$$\tilde{y} = [\Phi_f \ \Phi_{o,u}] \begin{bmatrix} \alpha_f \\ \alpha_{o,u} \end{bmatrix} + \omega \approx \Phi_{o,u} \alpha_{o,u} + \omega, \quad (8)$$

where Φ_f and $\Phi_{o,u}$ are the parts of Φ corresponding to the elements of α_f and $\alpha_{o,u}$. Note that we set $\alpha_f \approx 0$ in (8). BCS works based on the assumption that $\alpha_{o,u}$ is sparse, which is the case for our obstacle mapping. The vector $\alpha_{o,u}$ is then estimated using a maximum *a posteriori* (MAP) estimator and by using a prior distribution that preserves the sparsity of $\alpha_{o,u}$. Several prior distributions have been proposed in the literature [24], [25], [31]. In this paper, we assume a zero-mean Gaussian prior for $\alpha_{o,u}$. Such a prior is very simple to use and has been shown to achieve a sparse MAP estimate [25]. Conditioned on the channel measurements \tilde{y} and assuming uncorrelated Gaussian ω in (8), we have

$$p(\alpha_{o,u}|\tilde{y}) = \frac{p(\tilde{y}|\alpha_{o,u})p(\alpha_{o,u})}{\int p(\tilde{y}|\alpha_{o,u})p(\alpha_{o,u})d\alpha_{o,u}}, \quad (9)$$

where $p(\tilde{y}|\alpha_{o,u}) = \frac{1}{(2\pi)^{\frac{n_{o,u}}{2}} \sigma_0^{n_{o,u}}} \exp\left(-\frac{\|\tilde{y} - \Phi_{o,u} \alpha_{o,u}\|^2}{2\sigma_0^2}\right)$, $p(\alpha_{o,u}) = \frac{1}{(2\pi)^{\frac{n_{o,u}}{2}} |R_{o,u}|^{\frac{1}{2}}} \exp\left(-\frac{1}{2} \alpha_{o,u}^T R_{o,u}^{-1} \alpha_{o,u}\right)$, $n_{o,u}$ is the number of elements of $\alpha_{o,u}$ and $R_{o,u}$ is its covariance matrix. It can be easily shown that the posterior distribution $p(\alpha_{o,u}|\tilde{y})$ is also Gaussian in this case, i.e.,

$$p(\alpha_{o,u}|\tilde{y}) = \frac{1}{(2\pi)^{\frac{n_{o,u}}{2}} |\Sigma_{o,u}|^{\frac{1}{2}}} \exp\left(-\frac{1}{2} (\alpha_{o,u} - \hat{\alpha}_{o,u})^T \Sigma_{o,u}^{-1} (\alpha_{o,u} - \hat{\alpha}_{o,u})\right), \quad (10)$$

where

$$\hat{\alpha}_{o,u} = \frac{1}{\sigma_0^2} \Sigma_{o,u} \Phi_{o,u}^T \tilde{y}, \quad \Sigma_{o,u} = \left(\frac{1}{\sigma_0^2} \Phi_{o,u}^T \Phi_{o,u} + R_{o,u}^{-1} \right)^{-1}. \quad (11)$$

The vector $\hat{\alpha}_{o,u}$ is the MAP estimate of $\alpha_{o,u}$, which can be similarly partitioned as $\hat{\alpha}_{o,u} = [\hat{\alpha}_o^T \ \hat{\alpha}_u^T]^T$. Here, $\hat{\alpha}_o$ and $\hat{\alpha}_u$ are the estimated decay coefficients of the cells in \mathcal{I}_o and \mathcal{I}_u , respectively. Then, for every $k \in \mathcal{I}_u$ we have $\hat{x}_k = 1$ if $\hat{\alpha}_k > \alpha_{\text{th}}$, and $\hat{x}_k = 0$ otherwise.

Note that estimates of σ_0 and $R_{o,u}$ are needed to find the MAP estimate of $\alpha_{o,u}$ in (11). Next, we show how to estimate σ_0 and $R_{o,u}$ based on our channel measurements. The estimation of σ_0 is based on Expectation Maximization as is utilized in the BCS literature. As for $R_{o,u}$, an uncorrelated vector is assumed in the BCS literature. In our case of wireless-based obstacle mapping, if the spatial correlation is not considered, the sparsest map may not be the right one. In other words, it is important to consider the spatial correlation of the map when reconstructing based on sparse wireless measurements. We thus next show how we can have an estimate of the spatial correlation of the map.

A. Estimation of the Hyperparameters

Without loss of generality, we assume that indices of the elements of $\alpha_{o,u}$ are $1, \dots, n_{o,u}$. To account for the correlation of the cells, we assume the following form for $R_{o,u}$: $R_{o,u} = (\sigma_{o,u} \sigma_{o,u}^T) \otimes S_{o,u}$, where $\sigma_{o,u} = [\sigma_1, \dots, \sigma_{n_{o,u}}]^T$ is the vector of the standard deviations of the elements of $\alpha_{o,u}$ and $S_{o,u}$ is their correlation matrix. In general, finding a good model for the spatial correlation of the map is challenging due to its sparse structure. Based on our experience with several maps, an exponential correlation matrix results in a good reconstruction quality. Thus, we consider the following function in this paper: $[S_{o,u}]_{k_1, k_2} = \exp\left(-\frac{\|\xi_{cm, k_1} - \xi_{cm, k_2}\|}{\zeta}\right)$, for $1 \leq k_1, k_2 \leq n_{o,u}$. Here, $\xi_{cm, k}$ denotes the position of the center of the mass of the k^{th} cell. The correlation parameter ζ determines how correlated the elements of $\alpha_{o,u}$ are.

Note that due to the high quality of laser measurements, the uncorrelated assumption in laser mapping approach of Section III does not degrade the map reconstruction performance. However, considering the correlation of the cells is important when mapping the see-through parts of the workspace using the BCS method, as we indicated before.

Based on the proposed model, the hyperparameters to estimate are $\sigma_0, \dots, \sigma_{n_{o,u}}$ and ζ . Our proposed approach for estimating these hyperparameters is summarized into two steps:

- 1) Estimate the ζ a priori using a number of sample maps.
- 2) Estimate $\sigma_0, \dots, \sigma_{n_{o,u}}$ using expectation maximization (EM) and based on the estimated ζ from the previous step.

Next, we explain these two steps in more details.

1) *Estimation of the Correlation Parameter ζ* : In general, coming up with an estimate of the spatial correlation of an obstacle map is a challenging task. In this paper, we use a set of available obstacle maps to estimate ζ a priori. This estimate is then utilized in our obstacle mapping with real measurements. Consider a set \mathcal{X} which contains a number of binary maps. For every $x \in \mathcal{X}$, define the set $\mathcal{B}(x, d) \triangleq \{(k_1, k_2) \mid \|\xi_{cm, k_1} - \xi_{cm, k_2}\| - d \leq \epsilon\}$, for a small ϵ . The estimation of correlation at distance d is then given as follows:

$$\gamma(d) = \frac{\sum_{x \in \mathcal{X}} \sum_{(k_1, k_2) \in \mathcal{B}(x, d)} \neg(x_{k_1} \oplus x_{k_2})}{\sum_{x \in \mathcal{X}} |\mathcal{B}(x, d)|}, \quad (12)$$

where \oplus and \neg denote bitwise exclusive-or and negation. The estimate $\hat{\zeta}$ of ζ is then calculated by finding the best exponential fit to $\gamma(d)$ for a given vector of distances $D = [d_1, \dots, d_M]^T$. It can be easily confirmed that $\hat{\zeta} = -\frac{D^T \Gamma}{D^T D}$, where $\Gamma = [\log(\gamma(d_1)), \dots, \log(\gamma(d_M))]^T$.

2) *Estimation of $\sigma_0, \dots, \sigma_{n_{o,u}}$ using Expectation Maximization (EM)*: The EM approach provides an iterative method for estimating $\sigma_0, \dots, \sigma_{n_{o,u}}$ and has been used in the BCS literature. Let us define $\rho \triangleq (\sigma_0, \dots, \sigma_{n_{o,u}})$. Also, let $\hat{\rho}^\tau = (\hat{\sigma}_0^\tau, \dots, \hat{\sigma}_{n_{o,u}}^\tau)$ represent the estimates of ρ at iteration τ . We then have,

$$\text{E step: } \Theta(\rho | \hat{\rho}^\tau) = \mathbb{E}_{\alpha_{o,u} | \tilde{y}, \hat{\rho}^\tau} \left\{ \log \left[p(\tilde{y} | \alpha_{o,u}) p(\alpha_{o,u}) \right] \right\},$$

$$\text{M step: } \hat{\rho}^{\tau+1} = \arg \max_{\rho} \Theta(\rho | \hat{\rho}^\tau). \quad (13)$$

Let $\hat{\alpha}_{o,u}^\tau$ and $\hat{\Sigma}_{o,u}^\tau$ denote $\hat{\alpha}_{o,u}$ and $\Sigma_{o,u}$ in (11) when $\sigma_0, \dots, \sigma_{n_{o,u}}$ are replaced with $\hat{\sigma}_0^\tau, \dots, \hat{\sigma}_{n_{o,u}}^\tau$. After some

straightforward calculations, we then have the following:⁴

$$\begin{aligned} \Theta(\rho | \hat{\rho}^\tau) = & -n_w \log(\sigma_0) - \frac{1}{2} \log(|R_{o,u}|) \\ & - \frac{1}{2\sigma_0^2} \|\tilde{y} - \Phi_{o,u} \hat{\alpha}_{o,u}^\tau\|^2 - \frac{1}{2} (\hat{\alpha}_{o,u}^\tau)^T R_{o,u}^{-1} \hat{\alpha}_{o,u}^\tau \\ & - \frac{1}{2\sigma_0^2} \text{tr}(\Phi_{o,u}^T \Phi_{o,u} \hat{\Sigma}_{o,u}^\tau) - \frac{1}{2} \text{tr}(R_{o,u}^{-1} \hat{\Sigma}_{o,u}^\tau) + \text{const.} \end{aligned} \quad (14)$$

Maximizing $\Theta(\rho | \hat{\rho}^\tau)$ as a function of ρ is not straightforward for $\zeta > 0$. At this step, we sub-optimally assume that ζ is small.⁵ We can show that for $\zeta \rightarrow 0$, $R_{o,u}$ will be diagonal which results in the following update rules for ρ [25]:

$$\begin{aligned} \sigma_0^{\tau+1} &= \left[\frac{1}{n_w} \left(\text{tr}(\Phi_{o,u}^T \Phi_{o,u} \hat{\Sigma}_{o,u}^\tau) + \|\tilde{y} - \Phi_{o,u} \hat{\alpha}_{o,u}^\tau\|^2 \right) \right]^{1/2}, \\ \sigma_k^{\tau+1} &= \left[\frac{[\hat{\Sigma}_{o,u}^\tau]_{k,k} + [\hat{\alpha}_{o,u}^\tau]_k^2}{n_w} \right]^{1/2}, \quad k = 1, \dots, n_{o,u}. \end{aligned} \quad (15)$$

Note that although (15) is the true EM update rule, some authors suggested suboptimal update rules that have a faster convergence rate in the general context of BCS [25]. Algorithm 1 shows the steps involved in estimating the map using our integrated occupancy grid and BCS method.

Algorithm 1: Integrated Occupancy Grid Mapping and BCS for See-Through Mapping

Input: $z_{1:t}, u_{1:t-1}, \tilde{y}, \Phi, \alpha_{th}, \psi_{th}, \tau_{max}, \sigma_{init, comm}, \sigma_{init, cell}, \text{tol}, \mathcal{X}, \epsilon$

Output: Estimate of the binary map $\hat{x} = [\hat{x}_f^T \hat{x}_o^T \hat{x}_u^T]^T$
Using $z_{1:t}$ and $u_{1:t-1}$, calculate $\psi_{k,t}$, for all k , using the occupancy grid approach of Section III;

Calculate the set of indices $\mathcal{I}_f, \mathcal{I}_o$ and \mathcal{I}_u and rearrange the elements of x and α accordingly as $x = [x_f^T x_o^T x_u^T]^T$ and $\alpha = [\alpha_f^T \alpha_o^T \alpha_u^T]^T$;

Set elements of \hat{x}_f to zero and elements of \hat{x}_o to one;

Using a set of maps \mathcal{X} , calculate $\hat{\zeta}$ using the approach of Section IV-A1;

Set $\hat{\sigma}_0^0 = \sigma_{init, comm}$ and $\hat{\sigma}_k^0 = \sigma_{init, cell}$, for $k \in 1, \dots, n_{o,u}$, assuming that the indices of the elements of $\alpha_{o,u} = [\alpha_o^T \alpha_u^T]^T$ are $1, \dots, n_{o,u}$;

for $\tau \leftarrow 0$ **to** τ_{max} **do**

Calculate $\hat{\alpha}_{o,u}^\tau$ and $\hat{\Sigma}^\tau$ by substituting $\hat{\sigma}_0^\tau, \dots, \hat{\sigma}_{n_{o,u}}^\tau$ and $\hat{\zeta}$ in (11);

Calculate $\hat{\sigma}_0^{\tau+1}, \dots, \hat{\sigma}_{n_{o,u}}^{\tau+1}$ using (15) or the suboptimal update rule of [25] with a better convergence rate;

if $\max_{1 \leq k \leq n_{o,u}} \left| \log \frac{\hat{\sigma}_k^{\tau+1}}{\hat{\sigma}_k^\tau} \right| < \text{tol}$ **then**

| break;

end

end

From the most updated $\hat{\alpha}_{o,u}^\tau$, use $\hat{\alpha}_u^\tau$ and set $\hat{x}_u = U(\hat{\alpha}_u^\tau > \alpha_{th})$, where $U(\cdot)$ is the vector indicator function;

⁴Here we have used the fact that for a Gaussian α , with mean $\hat{\alpha}$ and covariance Σ , we have $\mathbb{E}\{R\alpha\} = R\hat{\alpha}$ and $\mathbb{E}\{\alpha^T R \alpha\} = \hat{\alpha}^T R \hat{\alpha} + \text{tr}(R\Sigma)$, for any positive definite R .

⁵Although we assume an uncorrelated map for the sake of estimating $\sigma_0, \dots, \sigma_{n_{o,u}}$, the estimate of ζ of Eq. 12 is used when calculating $\hat{\alpha}_{o,u}^\tau$ and $\hat{\Sigma}_{o,u}^\tau$.

V. INTEGRATION OF OCCUPANCY GRID MAPPING AND TOTAL VARIATION (TV) MINIMIZATION FOR MAPPING WITH SEE-THROUGH CAPABILITIES

So far we have discussed an integrated BCS and occupancy grid mapping approach for wireless-based obstacle mapping of hidden objects. In our past work, we have proposed a Total Variation framework for wireless-based mapping of hidden objects [17]–[19]. In this section, we briefly summarize our past work along this line and then discuss how to integrate it with occupancy grid mapping for the sake of completion. In the subsequent sections, we then compare the performance of the integrated occupancy grid/BCS-based and occupancy grid/TV-based approaches and discuss the underlying tradeoffs. As we discussed in Section I, the TV-based approach does not depend on estimating any underlying model parameters or assuming a specific model, which is an advantage over the BCS approach. However, the estimated variances of the BCS approach can provide a base for guiding the robots to the places which are better for collecting wireless measurements, as we propose later in Section VII. Thus, in this paper we consider integration based on both approaches and bring an understanding to the underlying tradeoffs.

TV minimization method works based on the fact that the gradient of typical obstacle maps is sparse. Several methods have been proposed in the literature for the reconstruction of general 2D signals based on this property [20], [32], [33]. TV minimization is one of such methods which is shown to be effective in restoring signals that have staircase characteristics [34]. Next, we explain this method in more detail.

Let f denote the vectorized version of an $M \times N$ matrix F . Define the following operators:

$$D_{h,i,j}(f) = \begin{cases} F_{i+1,j} - F_{i,j}, & i < M \\ F_{i,j} - F_{i,1}, & i = M \end{cases} \text{ and } D_{v,i,j}(f) = \begin{cases} F_{i,j+1} - F_{i,j}, & j < N \\ F_{i,j} - F_{i,1}, & j = N \end{cases}.$$

The TV function is defined as follows:

$$\text{TV}(f) = \sum_{i,j} \|D_{i,j}(f)\|, \quad (16)$$

where $D_{i,j}(f) = [D_{h,i,j}(f) \ D_{v,i,j}(f)]$, and the $\|\cdot\|$ operator can either represent the ℓ_1 norm, corresponding to the anisotropic discretization of TV, or the ℓ_2 norm, corresponding to the isotropic discretization of TV. Unless we specifically indicate otherwise, the results of this paper are based on using anisotropic TV. TV minimization method then solves the following problem or a variation of it:

$$\min_f \text{TV}(f), \text{ subject to } b = Af, \quad (17)$$

where b is the measurement vector, which is linearly related to f through a matrix A . The optimization problem of (17) can be proved to be convex. Several algorithms have been proposed to solve this problem efficiently [32], [33], [35]. In this paper we use the recently-proposed TVAL3 (TV minimization by augmented Lagrangian and alternating direction) algorithm [33]. TVAL3 iteratively minimizes the augmented Lagrangian of (17), which includes quadratic penalty terms that try to enforce the equality constraints [33]. We next explain how TVAL3 can be used for mapping the portion of the workspace that cannot be seen by the onboard laser scanners of the robots.

Without loss of generality, assume that the obstacle map of

interest is a rectangular map and α is the vectorized version of the 2D signal that represents the wireless decay coefficients of the cells on the grid. Using (17), we then propose the following integrated approach for estimating the parts of the map that have not been seen by the laser scanners of the robots:

- 1) The sets \mathcal{I}_f , \mathcal{I}_o and \mathcal{I}_u are found using the laser measurements and following the same approach of Section IV. We then set $\hat{x}_k = 0$ for $k \in \mathcal{I}_f$, and $\hat{x}_k = 1$ for $k \in \mathcal{I}_o$.
- 2) The laser measurement matrix Φ_{las} is formed. Each row of Φ_{las} has n elements and corresponds to a cell $k \in \mathcal{I}_f$, with its k^{th} element equal to one and the rest of its $n - 1$ elements equal to zero.
- 3) The estimate $\hat{\alpha}$ of α is then found by solving the following TV minimization problem using the TVAL3 algorithm:
$$\min_{\alpha} \text{TV}(\alpha), \text{ subject to } \begin{bmatrix} \tilde{y} \\ 0 \end{bmatrix} = \begin{bmatrix} \Phi \\ \Phi_{\text{las}} \end{bmatrix} \alpha. \quad (18)$$
- 4) For each $k \in \mathcal{I}_u$, we then set $\hat{x}_k = 1$ if $\hat{\alpha}_k > \alpha_{\text{th}}$, and $\hat{x}_k = 0$ otherwise.

Algorithm 2: Integrated Occupancy Grid Mapping and TV minimization for See-Through Mapping

Input: $z_{1:t}$, $u_{1:t-1}$, \tilde{y} , Φ , α_{th} and ψ_{th}

Output: Estimate of the binary map $\hat{x} = [\hat{x}_f^T \ \hat{x}_o^T \ \hat{x}_u^T]^T$

Using $z_{1:t}$ and $u_{1:t-1}$, calculate $\psi_{k,t}$, for all k , using the occupancy grid approach of Section III;

Calculate the set of indices \mathcal{I}_f , \mathcal{I}_o and \mathcal{I}_u and rearrange the elements of x and α accordingly as $x = [x_f^T \ x_o^T \ x_u^T]^T$ and

$\alpha = [\alpha_f^T \ \alpha_o^T \ \alpha_u^T]^T$;

Set elements of \hat{x}_f to zero and \hat{x}_o to one;

Form the laser measurement matrix Φ_{las} ;

Solve the TV minimization problem of (18) using a set of initial values for the Lagrange multipliers and α (the initial guess for α is usually the least square (LS) solution

$\alpha^0 = [\Phi^T \ \Phi_{\text{las}}^T] \begin{bmatrix} \Phi \Phi^T & \Phi_{\text{las}} \Phi^T \\ \Phi_{\text{las}} \Phi^T & \Phi_{\text{las}} \Phi_{\text{las}}^T \end{bmatrix}^{-1} \begin{bmatrix} \tilde{y} \\ 0 \end{bmatrix}$);

From the estimated $\hat{\alpha}$ pick $\hat{\alpha}_u$ and set $\hat{x}_u = U(\hat{\alpha}_u > \alpha_{\text{th}})$, where $U(\cdot)$ is the vector indicator function;

VI. COORDINATED VS. RANDOM WIRELESS CHANNEL MEASUREMENTS

The quality of our wireless-based sampling depends heavily on the positions from which the map is sampled. In our previous work we proposed two motion sampling strategies for wireless-based cooperative mapping based on TV minimization, namely *coordinated* and *random* approaches. We next briefly summarize these two approaches, which we will then extensively use for our integrated approaches. For more details on these motion sampling patterns in the context of TV-based wireless obstacle mapping, the readers are referred to [17], [19].

Consider the case where a pair of robots move outside the structure of interest in a coordinated fashion along the arrow at angle 0° as shown in Fig. 3 (left). If wireless measurements are taken at several places along that line such that at each position the line segment between the TX and RX robots representing the wireless ray (see dashed line in the figure) remains perpendicular to the 0° line, then we say that the robots are making coordinated measurements at angle 0° . The trajectories indicated by the arrows in Fig. 3 (left), are examples

of routes where coordinated measurements at angles 0° and 90° can be taken. Similar coordinated measurements can be made across any other angle.

Having the robots move in a coordinated way, however, may not be always possible due to environmental constraints. For instance, the path where the robots need to move for making coordinated measurements may be partially blocked. In such cases, the robots may have to make measurements at any location available to them without trying to maintain a specific pattern. As such, we also consider a *random* measurement case, where the robots make wireless measurements at randomly-chosen TX-RX positions. Fig. 3 (right) shows an example of such a case.

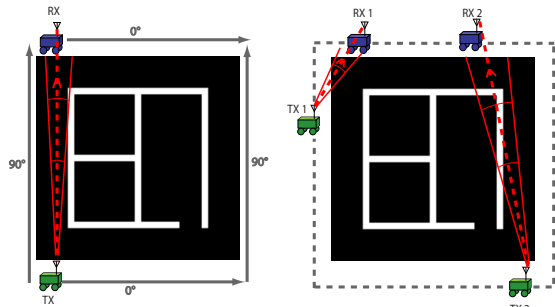


Fig. 3. An illustration of wireless-based obstacle mapping with (left) coordinated wireless measurements and (right) random wireless measurements.

In our previous work [19], we established that in general TV minimization with coordinated measurements provides a better reconstruction quality and see-through capability, as compared to TV minimization with random measurements, as long as jump angles are sampled [19]. It now becomes pertinent to understand how BCS compares to TV minimization in the context of both random and coordinated measurements. We start by comparing the performance of the BCS-based and TV-based approaches in a simulation environment where we can test more scenarios. We then present our experimental results in Section VIII.

Suppose that a pair of robots are trying to map the structure in Fig. 13 (a). For the coordinated case, the robots move in parallel along routes outside of the structure. Figure 3 (left) shows the routes where the robots move to make measurements along 0° and 90° routes. As the number of measurements increases, the robots make measurements along more angles, which are chosen so as to make the angle distribution as uniform as possible, while keeping the previously-chosen angles. For the random case, the robots make measurements at random positions along the dashed lines of Fig. 3 (right) without following a specific pattern.

In order to motivate our discussion, we start by comparing the performance of these approaches for a noiseless case, i.e. when $\omega_{i,j,t}$ of Eq. 1 is equal to zero. In this example, we assume that the positions of the robots are known at any time and that the reconstruction is based only on wireless measurements, i.e. no probabilistic grid mapping is used. We show the results as a function of the wireless sampling rate, where each sampling rate denotes the total number of wireless transmissions divided by the size of the 2D map in pixels (in percentage). In this example, the size of the map is 64 by 64 pixels and the following

underlying parameters are used: $\alpha_{th} = 0.2$, $\sigma_{init,comm} = 0$, $\sigma_{init,cell} = 1$, $\hat{\zeta} = 0.2$, $\tau_{max} = 150$ and $tol = 0.001$ (see Algorithm 1 for more on tol). We discuss how we estimate the initial values of the underlying parameters for the BCS approach when we present our experimental results in Section VIII.

Figure 4 shows the reconstruction using only 10% of measurements. As can be seen, TV minimization with coordinated measurements results in a perfect reconstruction. Furthermore, similar to TV minimization, BCS coordinated also has a smaller Normalized Mean Squared Error (NMSE) than BCS random. As Fig. 5 shows, by increasing the number of measurements to 15%, a significant increase in the reconstruction quality of BCS coordinated is observed. For both cases (BCS and TV minimization), the coordinated approaches outperform the random ones. Furthermore, *for the random strategy, BCS has a better reconstruction quality than TV minimization*. Fig. 6 (left) confirms the same trend in the noiseless case, for a range of percentage measurements.

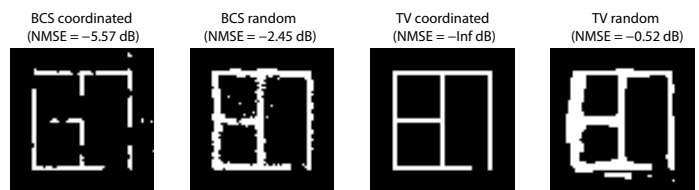


Fig. 4. The reconstruction of the obstacle of Fig. 13 (a) using 10% noiseless simulated measurements.

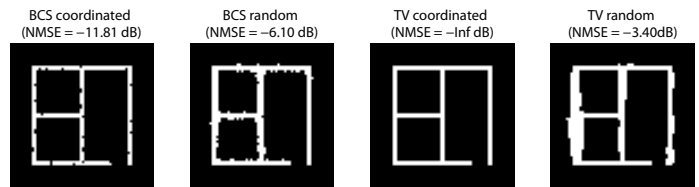


Fig. 5. The reconstruction of the obstacle of Fig. 13 (a) using 15% noiseless simulated measurements.

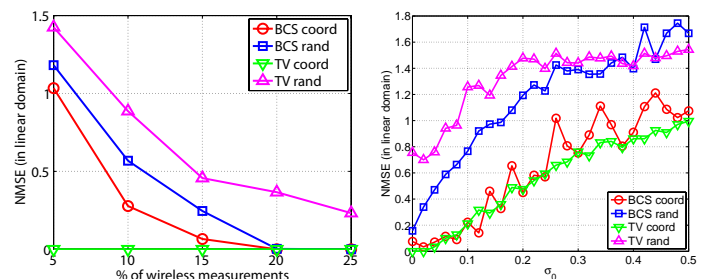


Fig. 6. (left) NMSE versus the percentage of wireless measurements in the noiseless case for the reconstruction of the obstacle of Fig. 13 (a); (right) NMSE versus σ_0 for the reconstruction of the obstacle of Fig. 13 (a) with 15% simulated wireless measurements.

Next, we consider the impact of noise. As we indicated in the wireless channel measurement model of Eq. 8, the elements of ω are taken to be uncorrelated Gaussian random variables with the variance σ_0^2 . We furthermore showed that this assumption does indeed provide a good match with the data obtained using our experimental robotic platform. We next show the effect of such noise in a simulation environment with the same parameters as before except for: $\tau_{max} = 500$ and $\sigma_{init,comm} = \sigma_0$.

Figure 7 shows the mapping performance using 15% noisy measurements with $\sigma_0 = 0.1$. As can be seen, similar to the

noiseless case, the coordinated approaches provide a better reconstruction quality than the random ones. Furthermore, TV minimization with random measurements has the worst performance for this sample noise variance. Fig. 6 (right) then shows the NMSE as a function of σ_0 . It can be seen that similar trends hold in this figure except at very high values of σ_0 where the random TV starts outperforming the random BCS. However, the reconstruction quality at such high level of noise may not be acceptable anymore for both cases.

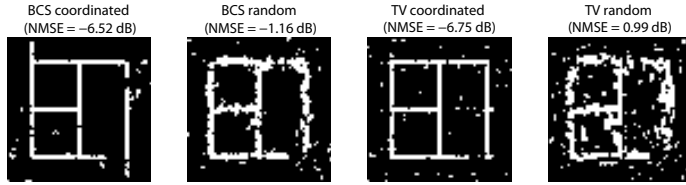


Fig. 7. The reconstruction of the obstacle of Fig. 13 (a) using 15% noisy simulated wireless measurements ($\sigma_0 = 0.1$).

VII. AN ADAPTIVE DATA COLLECTION STRATEGY FOR INTEGRATED OBSTACLE MAPPING

So far, we have assumed that the laser and wireless channel measurements are collected through either random or coordinated motion patterns, without an online optimization of the data collection process. The trajectories can further be adapted online to better collect laser or wireless channel measurements based on a feedback from the current mapping quality. Online motion optimization for occupancy grid mapping, using laser measurements, has been extensively studied in the robotics literature. Examples include next-best-view (NBF) [36] and frontier-based [37], [38] algorithms. However, online motion adaption based on a feedback from the current mapping quality for wireless-based see-through mapping has not been studied before. In this section, we propose an adaptive strategy for collecting wireless channel measurements that aims to improve the see-through performance of either BCS or TV minimization methods.

Consider the obstacle-free part of the workspace $\mathcal{W}_f \subset \mathcal{W}$, estimated using the occupancy grid approach of Section III. Without loss of generality, assume that there exists only one pair of TX and RX robots. Let $\mathcal{P} \subset \mathcal{W}_f$ denote the set of possible positions where the robots can be. For instance, \mathcal{P} could be the set of positions along the rectangle that surrounds the workspace (see the dashed line of Fig. 3 (right) for an example). Consider the wireless channel measurements available to the robots at time t . These channel measurements include the channel measurements collected by the robots along their trajectories up to time t , and possibly a set of *a priori* channel measurements available at the beginning of the operation. The idea is to choose the next best positions of the robots such that the new channel measurement at time $t + 1$ is the most informative, given the past measurements.

We specifically propose two adaptive approaches: *ad-hoc* and *variance-based*. The ad-hoc approach can be used to adaptively collect wireless measurements in both BCS and TV minimization methods. The variance-based approach, on the other hand, uses the estimated variance of the BCS case and is therefore only applicable to the BCS method.

Let Φ_t denote the measurement matrix found based on the available wireless channel measurements up to time step t .

Also let $\Phi_{o,u,t}$ denote the part of Φ_t that corresponds to the occupied and unknown cells whose indices are in the set $\mathcal{I}_{o,u}$, which is given at the end of the occupancy grid mapping operation. Additionally, let $\hat{\Sigma}_{o,u,t}$ represent the estimated covariance matrix $\Sigma_{o,u}$ in the BCS method, calculated based on the available wireless channel measurements up to time t . The column vector of the diagonal elements of $\hat{\Sigma}_{o,u,t}$ is then shown by $\text{diag}(\hat{\Sigma}_{o,u,t})$. At any time t , the set of admissible pairs of positions for the RX and TX robots is a subset of $\mathcal{P} \times \mathcal{P}$ defined as follows:

$$\mathcal{F}_t \triangleq \left\{ (p_1, p_2) \in \mathcal{P} \times \mathcal{P} \mid \|\xi_{i,t} - p_i\| \leq d_{\max}, \right. \\ \left. i = 1, 2, \text{ dir. antennas can be aligned along } \mathcal{L}(p_1, p_2) \right\}, \quad (19)$$

where d_{\max} is the maximum step size of the robots and $\mathcal{L}(p_1, p_2)$ denote the line segment between p_1 and p_2 . Note that due to possible constraints on the rotation of the onboard antennas of the robots, some of the points may not be feasible and need to be excluded from the set of admissible points. For any pair of positions $(p_1, p_2) \in \mathcal{F}_t$ we then propose the following ad-hoc and variance-based next position optimization problem:

- Ad-hoc:

$$(\xi_{1,t+1}, \xi_{2,t+1}) = \underset{(p_1, p_2) \in \mathcal{F}_t}{\text{argmax}} \phi_{o,u}^T(p_1, p_2) \exp(-\Phi_{o,u,t}^T \mathbf{1}), \quad (20)$$
- Variance-based:

$$(\xi_{1,t+1}, \xi_{2,t+1}) = \underset{(p_1, p_2) \in \mathcal{F}_t}{\text{argmax}} \phi_{o,u}^T(p_1, p_2) \text{diag}(\hat{\Sigma}_{o,u,t}), \quad (21)$$

where $\Phi_{o,u,t}^T \mathbf{1}$ denotes the column vector of the column-sum of matrix $\Phi_{o,u,t}$ and $\phi_{o,u}(p_1, p_2)$ denotes the column vector corresponding to the parts of $\phi(p_1, p_2)$ that are in $\mathcal{I}_{o,u}$. The intuition behind the ad-hoc strategy is that the new measurement vector ($\phi^T(\xi_{1,t+1}, \xi_{2,t+1})$) should have a small correlation with the existing measurement vectors, i.e. rows of Φ_t . This will increase the probability that the new wireless measurement (the line segments between the TX and RX robots) hits the cells that are not yet visited. We have further found that amplifying the impact of the unvisited cells by using the exponential function can improve the performance. The ad-hoc strategy (20) then chooses the pair whose connecting line segment passes through the cells that have previously been visited the least. This strategy can be used with both BCS and TV. The variance-based optimization function of (21), on the other hand, is based on the summation of the variances of the cells that the new wireless measurement line hits and thus can only be used by BCS. The new measurement line is then chosen such that the cells with high variances (high uncertainty) are selected.

We next show the performance of our online adaption integrated mapping framework in a simulation environment. Consider the case where the robots are trying to reconstruct the obstacle map of Fig. 13 (a) based on only noiseless wireless measurements.

Assume that no occupancy grid mapping is performed, i.e. $\Phi_t = \Phi_{o,u,t}$ for all t . For this example, we let \mathcal{P} correspond to a set of discrete positions along the square dashed line that surrounds the map of interest (see Fig. 3 (right)). The size of

the map is 64×64 pixels. Thus, we let the admissible positions be evenly distributed along the dashed line such that $\text{card}(\mathcal{P}) = 256$. We also set $\mathcal{F}_t \triangleq \{(p_1, p_2) \in \mathcal{P} \times \mathcal{P}\}$.

At the beginning of the operation, the robots make a very small number of random wireless measurements, corresponding to 3% of the map. The reconstruction of BCS and TV minimization using these initial measurements is shown in Fig. 8. For BCS, the same parameters of the example of Fig. 6 (left) are used. The robots then proceed to make additional wireless measurements based on our online adaptive approach, choosing the next best positions out of \mathcal{F}_t . We assume that d_{\max} is infinite and that any pair of positions can be selected from \mathcal{F}_t . Fig. 9 shows the quality of adaptive mapping after 15% measurements are adaptively collected. As can be seen, the mapping quality has improved considerably. It can furthermore be seen that, while the ad-hoc methods result in an acceptable reconstruction quality, the variance-based approach slightly outperforms the ad-hoc strategies, as expected. Figure 10 shows the mapping performance curves as a function of the percentage of the additional wireless measurements. As can be seen, BCS approaches perform better than TV and the variance-based approach has a slight performance gain over the ad-hoc one.

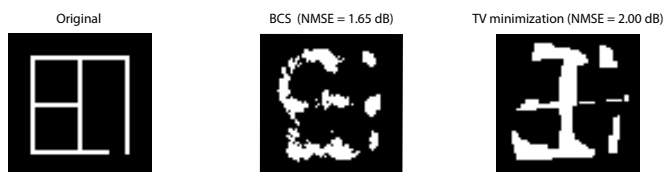


Fig. 8. Initial reconstruction of the obstacle of Fig. 13 (a) based on 3% noiseless simulated wireless measurements.

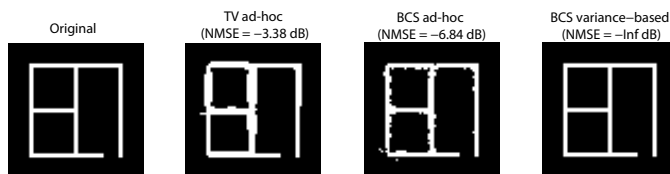


Fig. 9. The reconstruction of the obstacle of Fig. 13 (a) after 15% additional adaptive wireless measurements are collected.

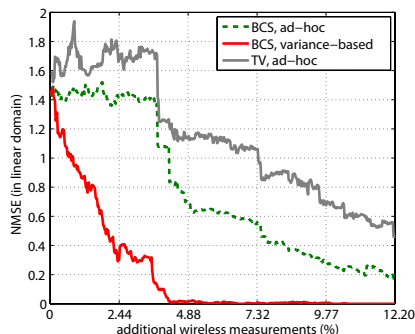


Fig. 10. NMSE as a function of the percentage of the additional wireless measurements for our adaptive path planning strategy, in reconstructing the whole map of Fig. 13 (a) (3% initial random measurements were used).

VIII. EXPERIMENTAL RESULTS

So far we have proposed two approaches for integrating occupancy grid mapping (using laser measurements) with CS mapping (using wireless channel measurements). In this section,

we show the performance of our proposed framework in the reconstruction of a real occluded structure that can not be mapped with any of the existing techniques in the literature. We start by describing our experimental robotic setup.

A. Summary of the Experimental Setup

Our setup consists of two Pioneer P3-AT mobile robots [39]. We equipped each robot with a directional narrow-beam antenna from Laird with horizontal and vertical beamwidths of 21° and 17° , respectively. As we have shown in our previous work [28], the use of narrow-beam antennas is crucial in order to limit the impact of multipath fading. We have also developed a servo mechanism for antenna rotation and control, which allows the antennas of the TX and RX robots to remain aligned throughout the experiment. Each antenna is connected to an IEEE 802.11g wireless card and can record the received RSSI as the robots move. Additionally, we equipped each robot with a Hokuyo URG laser scanner which has a maximum range of 5.6 m and a scanning angle of 240° . Figure 11 (left) shows the resulting platform with the laser scanner and the directional antenna. Figure 11 (right) shows the robots making wireless measurements in order to see through the walls and reconstruct the obstacle inside while the onboard laser scanners are used to map the portions of the workspace that can be directly seen by the laser scanners.



Fig. 11. (left) A Pioneer P3-AT robot equipped with our servo control mechanism/fixture, adaptive narrow-beam directional antenna and Hokuyo laser scanner; (right) two robots using laser scanners and wireless measurements in order to map an obstacle structure that includes occluded parts.

We have developed two separate software packages for our experiments. The first one is for motion planning and occupancy grid mapping using laser scanners. This software package is developed in C++ under Linux and makes use of the Robot Operating System (ROS) [40] for controlling the Pioneer P3-AT platform (using `p2os` stack), operating the Hokuyo URG laser scanner (using `hokuyo_node` laser driver) and implementing SLAM (using the `gmapping` stack). The second software package is used for collecting the RSSI measurements between the two robots as they move along their trajectories. More details on this software package can be found in [28].

We then implement our integrated framework in MATLAB by using the RSSI data collected by the robots and the occupancy grid map that is given by the SLAM algorithm to build the entire map of the structure.

B. Experimental Results for Mapping a Structure with Occluded Parts

We next show the performance and see-through capabilities of our proposed integrated approach in mapping an obstacle

structure that has occluded parts. Figure 12 (left) shows a structure with its horizontal cut shown in the right figure. First, consider the case where a robot only uses its laser scanner outside of the structure as far as it can get using the entrance on the lower right side. In order to avoid the laser scanner falsely detecting the antenna as an obstacle, we set the gmapping algorithm to discard any laser reading beyond the range -60° to 60° (with respect to the robot frame). Fig. 13 (b) shows the resulting generated map. As can be seen, the existence, position and dimensions of the occluded parts can not be determined by the laser scanner, as expected. Thus, we let the robots do a few random wireless measurements from the positions along the dashed trajectories of Fig. 12 (right) and apply our proposed integrated approach.⁶ The following parameters are used for the BCS case: $\alpha_{th} = 7$, $\sigma_{init,comm} = 10.34$. The rest of the parameters are the same as in Section VI. As pointed out before, we estimated $\zeta = 0.2$ by using several existing real maps a priori and applying Eq. 12. We consistently found that BCS is not as sensitive to the initialization of $\sigma_{init,cell}$ and therefore we have fixed it to a small value of one. As for $\sigma_{init,comm}$, we have used a priori wireless measurements with other structures that we have constructed in the past and estimated ω_{dB} by subtracting the impact of the structure to measure samples of the noise as illustrated in Fig. 2. We then calculated the standard deviation of this noise.

Subfigures (e) and (f) of Fig. 13 show the performance of our proposed integrated approach with BCS and TV minimization respectively. As can be seen, even at the very low sampling rate of 18% of the unknown part, corresponding to 6% of the overall map, the occluded wall (occluded to the laser scanners) can be clearly seen. The unknown part refers to the area where the laser scanner can not see the obstacles as marked in Fig. 13 (b). 18% wireless measurements is then the percentage of the wireless measurements as compared to the total number of the pixels of the unknown part. This percentage translates to 6% of the overall map, which is fairly small. It can be seen that the robots can map the structure with our integrated approach. Furthermore, it can be observed that random BCS performs better than random TV as we expected from the simulation results of the previous section. For the sake of comparison, Fig. 13 (c) and (d) show the reconstruction if we only use the collected wireless measurements (6% wireless measurements), without integration with the laser scanner data. As can be seen, it is hard to map this structure based on only 6% wireless measurements that are randomly collected from the dashed line of Fig. 12 (right), which motivates the use of the integrated approach.⁷

In summary, our experimental results show that the proposed integrated framework can map a more complex occluded structure that can not be mapped with existing strategies in the literature. Furthermore, both integrated TV and BCS-based approaches provide comparable reconstruction results, with the BCS-based approach performing better with random measure-

⁶Note that the robots make wireless measurements when positioned on the dashed line of Fig. 12 (right) in our experiment. If one robot transmits from inside the structure (using the entrance on the lower-right corner), better reconstructions can be achieved.

⁷Note that the case where both TX and RX are on the same side of the structure is naturally excluded from the possible set of TX/RX positions.

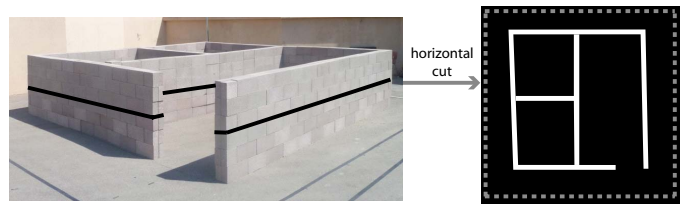


Fig. 12. (left) The obstacle structure of interest and (right) its horizontal cut. The paths where the robots can make random wireless measurements are marked with dashed lines in the right figure.

ments and TV-based approach with coordinated measurements. However, integrated BCS-based approach requires estimating the underlying model parameters as compared to the TV-based approach. This needs an initial estimation of the model parameters, which can be prone to errors. Thus, depending on the system requirements, the integrated mapping choice that is more suitable can be selected in practice.

IX. CONCLUSIONS AND FUTURE EXTENSIONS

In this paper we considered the problem of obstacle/object mapping using a team of mobile robots. We considered a scenario where each robot is equipped with a laser scanner, a wireless communication device and a directional antenna. We proposed an integrated framework for mapping with see-through capabilities based on both laser and wireless channel measurements. We specifically showed how to integrate occupancy grid mapping with two CS-based reconstruction methods: Bayesian compressive sensing (BCS) and total variation (TV) minimization. We compared the performance of these two approaches using both simulated and real data from our robotic platforms. For instance, our results indicated that the integrated BCS-based method is more appropriate for mapping based on random wireless measurements while TV-based integrated approach performs better with coordinated wireless measurements. The integrated BCS-based approach furthermore provides an estimate of the current mapping variance, which is more informative in general or can specifically be used for adaptive path planning and wireless measurement collection. It, however, requires an initial estimation of the underlying model parameters. Our experimental robotic testbed confirmed that the proposed integrated framework can map a more complex occluded structure that can not be mapped with existing strategies in the literature. We finally proposed an adaptive path planning strategy that utilizes the current estimate of uncertainty to better guide the robots for wireless measurement collection. Evaluation of the performance of our adaption strategies in mapping real obstacles is a subject of our future work.

REFERENCES

- [1] S. Thrun, W. Burgard, and D. Fox., *Probabilistic Robotics*. Cambridge, MA: MIT Press, 2005.
- [2] S. Thrun, "Robotic Mapping: A Survey," in *Exploring Artificial Intelligence in the New Millenium*. Morgan Kaufmann, 2002.
- [3] H. Durrant-Whyte and T. Bailey, "Simultaneous localization and mapping (SLAM): Part I," *IEEE Robotics & Automation Magazine*, vol. 13, no. 2, pp. 99–110, June 2006.
- [4] T. Bailey and H. Durrant-Whyte, "Simultaneous localization and mapping (SLAM): Part II," *IEEE Robotics & Automation Magazine*, vol. 13, no. 3, pp. 108–117, 2006.
- [5] S. Thrun, "Learning Occupancy Grids With Forward Sensor Models," *Autonomous Robots*, vol. 15, pp. 111–127, 2002.

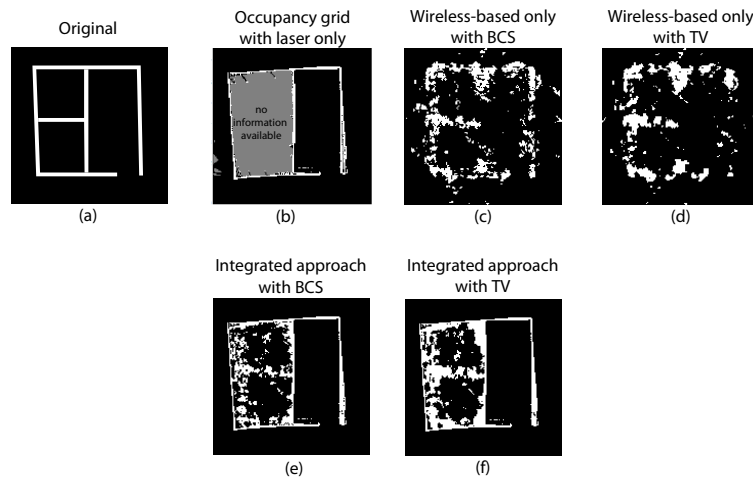


Fig. 13. (a) Horizontal cut of the obstacle map of Fig. 12, (b) occupancy grid mapping with laser scanners, reconstruction using wireless measurements with (c) BCS and (d) TV minimization, our proposed integrated framework with (e) BCS and (f) TV minimization. The percentage of wireless measurements is 18% of the unknown part, which corresponds to 6% of the overall map.

- [6] M. A. Paskin and S. Thrun, "Robotic mapping with polygonal random fields," in *Proceedings of the 21st Conference on Uncertainty in Artificial Intelligence*. AAAI Press, Arlington, VA, July 2005.
- [7] S. Thrun, W. Burgard, D. Fox, H. Hexmoor, and M. Mataric, "A Probabilistic Approach to Concurrent Mapping and Localization for Mobile Robots," in *Machine Learning*, 1998, pp. 29–53.
- [8] F. Dellaert, F. Alegre, and E. B. Martinson, "Intrinsic localization and mapping with 2 applications: Diffusion mapping and macro polo localization," in *IEEE Intl. Conf. on Robotics and Automation*, vol. 2, 2003, pp. 2344 – 2349.
- [9] R. Sim, G. Dudek, and N. Roy, "A Closed Form Solution to the Single Degree of Freedom Simultaneous Localisation and Map Building (SLAM) problem," in *IEEE Conf. on Decision and Control*, vol. 1, 2000, pp. 191–196.
- [10] M. W. M. G. Dissanayake, P. Newman, S. Clark, H. Durrant-Whyte, and M. Csorba, "A Solution to the Simultaneous Localization and Map Building (SLAM) Problem," *IEEE Transactions on Robotics and Automation*, vol. 17, no. 3, pp. 229–241, June 2001.
- [11] M. Montemerlo, S. Thrun, D. Koller, and B. Wegbreit, "FastSLAM: A Factored Solution to the Simultaneous Localization and Mapping Problem," in *Proceedings of the AAAI National Conference on Artificial Intelligence*. AAAI, 2002, pp. 593–598.
- [12] —, "FastSLAM 2.0: An Improved Particle Filtering Algorithm for Simultaneous Localization and Mapping that Provably Converges," in *Proceedings of the Sixteenth International Joint Conference on Artificial Intelligence (IJCAI)*. Acapulco, Mexico: IJCAI, 2003.
- [13] K. Murphy, "Bayesian Map Learning in Dynamic Environments," in *Advances in Neural Info. Proc. Systems (NIPS)*, San Mateo, CA, 1999, pp. 1015–1021.
- [14] G. Grisetti, C. Stachniss, and W. Burgard, "Improved Techniques for Grid Mapping With Rao-Blackwellized Particle Filters," *IEEE Transactions on Robotics*, vol. 23, no. 1, pp. 34–46, Feb. 2007.
- [15] Y. Mostofi and P. Sen, "Compressive Cooperative Mapping in Mobile Networks," in *Proceedings of the 28th American Control Conference (ACC)*, St. Louis, MO, June 2009, pp. 3397–3404.
- [16] Y. Mostofi, "Compressive Cooperative Sensing and Mapping in Mobile Networks," *IEEE Transactions on Mobile Computing*, vol. 10, no. 12, pp. 1769–1784, Dec. 2011.
- [17] Y. Mostofi and A. Gonzalez-Ruiz, "Compressive Cooperative Obstacle Mapping in Mobile Networks," in *Proceedings of the 29th Military Communications Conference (Milcom)*, San Jose, CA, Nov. 2010, pp. 947–953.
- [18] Y. Mostofi, "Compressive Cooperative Obstacle/Object Mapping and See-Through Capabilities in Robotic Networks," *IEEE Transactions on Mobile Computing*, vol. 12, no. 5, pp. 817–829, May 2013.
- [19] A. Gonzalez-Ruiz and Y. Mostofi, "Cooperative Robotic Structure Mapping Using Wireless Measurements – A Comparison of Random and Coordinated Measurements," 2013, accepted to appear, *IEEE Sensors Journal*.
- [20] E. Candès, J. Romberg, and T. Tao, "Robust uncertainty principles: exact signal reconstruction from highly incomplete frequency information," *IEEE Trans. on Information Theory*, vol. 52, no. 2, pp. 489–509, February 2006.
- [21] D. L. Donoho, "Compressed sensing," *IEEE Transactions on Information Theory*, vol. 52, no. 4, pp. 1289–1306, April 2006.
- [22] J. Wilson and N. Patwari, "Radio tomographic imaging with wireless networks," *IEEE Transactions on Mobile Computing*, vol. 9, no. 5, pp. 621–632, may 2010.
- [23] M. Kansa and M. Rabbat, "Compressed RF tomography for wireless sensor networks: Centralized and decentralized approaches," in *IEEE Intl. Conference on Distributed Computing in Sensor Systems*, June 2009.
- [24] S. Ji, Y. Xue, and L. Carin, "Bayesian Compressive Sensing," *IEEE Trans. on Signal Processing*, vol. 56, no. 6, pp. 2346–2356, June 2008.
- [25] M. E. Tipping, "Sparse Bayesian Learning and the Relevance Vector Machine," *J. Mach. Learn. Res.*, vol. 1, pp. 211–244, Sep. 2001.
- [26] S. Ji, Y. Xue, and L. Carin, "Bayesian compressive sensing," *IEEE Trans. on Signal Processing*, vol. 56, no. 6, pp. 2346–2356, June 2008.
- [27] A. Goldsmith, *Wireless Communications*. Cambridge University Press, 2005.
- [28] A. Gonzalez-Ruiz, A. Ghaffarkhah, and Y. Mostofi, "A Comprehensive Overview and Characterization of Wireless Channels for Networked Robotic and Control Systems," *Journal of Robotics*, vol. 2011, 2011.
- [29] Y. Mostofi, A. Gonzalez-Ruiz, A. Ghaffarkhah, and D. Li, "Characterization and Modeling of Wireless Channels for Networked Robotic and Control Systems - A Comprehensive Overview," in *Proceedings of 2009 IEEE/RSJ International Conference on Intelligent Robots and Systems (IROS)*, St. Louis, MO, October 2009.
- [30] H. Hashemi, "A Study of Temporal and Spatial Variations of the Indoor Radio Propagation Channel," in *5th IEEE International Symposium on Personal, Indoor and Mobile Radio Communications, 1994. Wireless Networks - Catching the Mobile Future*, vol. 1, Sept. 1994, pp. 127–134.
- [31] L. He and L. Carin, "Exploiting Structure in Wavelet-Based Bayesian Compressive Sensing," *IEEE Transactions on Signal Processing*, vol. 57, no. 9, pp. 3488–3497, Sept. 2009.
- [32] " ℓ_1 magic toolbox," <http://www.acm.caltech.edu/llmagic/>.
- [33] C. Li, "An efficient algorithm for total variation regularization with applications to the single pixel camera and compressive sensing," Ph.D. dissertation, RICE University, 2009.
- [34] D. Strong and T. Chan, "Edge-preserving and scale-dependent properties of total variation regularization," *Inverse Problems*, vol. 19, no. 6, p. S165, 2003.
- [35] Y. Wang, J. Yang, W. Yin, and Y. Zhang, "A new alternating minimization algorithm for total variation image reconstruction," *SIAM J. on Imaging Sciences*, vol. 1, no. 3, p. 248272, 2008.
- [36] H. H. H. Gonzalez-Banos and J.-C. Latombe, "Navigation Strategies for Exploring Indoor Environments," *The International Journal of Robotics Research*, vol. 21, no. 10-11, pp. 829–848, Oct. 2002.
- [37] D. Fox, J. Ko, K. Konolige, B. Limketkai, D. Schulz, and B. Stewart, "Distributed multi-robot exploration and mapping," *Proceedings of the IEEE*, 2006.
- [38] W. Burgard, M. Moors, C. Stachniss, and F. Schneider, "Coordinated Multi-Robot Exploration," *IEEE Transactions on Robotics*, vol. 21, pp. 376–386, 2005.
- [39] Adept Mobilerobots: http://www.mobileroobots.com/Mobile_Robots.aspx.
- [40] Robot Operating System (ROS): <http://www.ros.org/wiki/>.



Alejandro Gonzalez-Ruiz received the B.S. degree in electronics engineering from the Universidad del Valle de Guatemala, Guatemala City, Guatemala, in 2006, and the M.S. and Ph.D. degrees in electrical engineering from the University of New Mexico, Albuquerque, NM, USA, in 2009 and 2012, respectively.

From 2006 to 2007 he was with TECO Energy, Guatemala. From August 2012 to March 2013 he was a visiting researcher at the Department of Electrical and Computer Engineering at the University of California Santa Barbara, Santa Barbara, CA, USA. His research interests include compressive and cooperative sensing and control, through-the-wall mapping, and wireless

communications.

He was a recipient of a scholarship from TECO Energy for his undergraduate studies in 2001, and a Fulbright scholarship in 2007.



Alireza Ghaffarkhah received the B.S. and M.S. degrees in electrical engineering from Sharif University of Technology, Tehran, Iran, in 2005 and 2007, respectively. He completed his Ph.D. in electrical and computer engineering at the University of New Mexico, Albuquerque in 2012.

In 2012 he was a visiting researcher at the University of California Santa Barbara. His research interests include motion planning and control of robotic and mobile sensor networks, control and decision under communication constraints, and hardware/software design for robotic

systems. He is now a software engineer at Google.



Yasamin Mostofi received the B.S. degree in electrical engineering from the Sharif University of Technology, Tehran, Iran, in 1997, and the M.S. and Ph.D. degrees in the area of wireless communication systems from Stanford University, California, in 1999 and 2004, respectively. She is currently an associate professor in the Department of Electrical and Computer Engineering at the University of California Santa Barbara.

Dr. Mostofi is the recipient of the Presidential Early Career Award for Scientists and Engineers (PECASE), the National Science Foundation (NSF) CAREER award, the IEEE 2012 Outstanding Engineer Award of Region 6, and the Bellcore fellow-advisor award from the Stanford Center for Telecommunications in 1999, among other awards. Her research is multi-disciplinary and on mobile sensor networks. Current research thrusts include communication-aware navigation and decision making in robotic networks, compressive sensing and control, obstacle mapping, robotic routers, and cooperative information processing. She has served on the Control Systems Society conference editorial board since 2008.